Rev. Adv. Mater. Sci. 35 (2013) 48-58

KINETICS OF GRAIN BOUNDARY SLIDING AND ROTATIONAL DEFORMATION IN NANOCRYSTALLINE MATERIALS

I. A. Ovid'ko[1,2,3] and A.G. Sheinerman[1,2]

[1]Department of Mathematics and Mechanics, St. Petersburg State University, Universitetskii pr. 28, Staryi Peterhof, St. Petersburg 198504, Russia
[2]Institute of Problems of Mechanical Engineering, Russian Academy of Sciences, Bolshoj 61, Vasil. Ostrov, St. Petersburg 199178, Russia
[3]St. Petersburg State Polytechnical University, St. Petersburg 195251, Russia

Received: September 1, 2013

Abstract. Kinetics of combined grain boundary (GB) sliding and rotational deformation processes in nanocrystalline materials is examined using computer simulations of GB dislocation slip and climb. We consider the situation where GB sliding and rotational deformation (plastic deformation accompanied by crystal lattice rotations) serve as dominant deformation modes in a nanocrystalline specimen and thereby crucially influence its deformation behavior. Based on the results of the computer simulations, the dependences of the flow stress on plastic strain in nanocrystalline Ni and Al_2O_3 are calculated, and their strain rate sensitivity parameters are estimated. It was found that combined actions of GB sliding and rotational deformation modes enhance ductility of nanocrystalline specimens.

1. INTRODUCTION

Nanocrystalline metallic and ceramic materials (hereinafter called nanomaterials) are typically characterized by superior strength and show deformation behavior controlled by specific deformation mechanisms [1–23]. Thus, in parallel with conventional lattice slip (dominating in coarse-grained polycrystals), specific GB deformation mechanisms effectively operate in nanocrystalline materials. These include GB sliding, GB diffusional creep (Coble creep), stress-driven GB migration, twin deformation initiated at GBs, and rotational deformation mode conducted by GB defects [1,4,5,14]. In particular, GB sliding and other GB deformation mechanisms significantly or even dominantly contribute to plastic flow in both nanomaterials with finest grains (of sizes $\leq$20 nm) in wide temperature ranges and nanomaterials with intermediate grains (of sizes ranging from approximately 20 to 100 nm) exhibiting superplasticity at elevated temperatures [1,4,5,14].

The crucial aspect for (super)plastic deformation carried by GB sliding is in its accommodation at triple junctions of GBs [1,4]. For evident geometric reasons, triple junctions stop GB sliding and thereby serve as sites where plastic strain incompatibilities are produced in nanomaterials. These strain incompatibilities create high local stresses capable of initiating cracks, in which case cracks typically form at triple junctions in deformed nanomaterials [1,24–26]. In the context discussed, in order to control/avoid formation of dangerous strain incompatibilities, it is critically important to understand the micromechanisms for accommodation of GB sliding at triple junctions.

It is conventionally viewed that GB sliding in nano- and microcrystalline materials under

Corresponding author: I.A. Ovid'ko, e-mail: ovidko@nano.ipme.ru

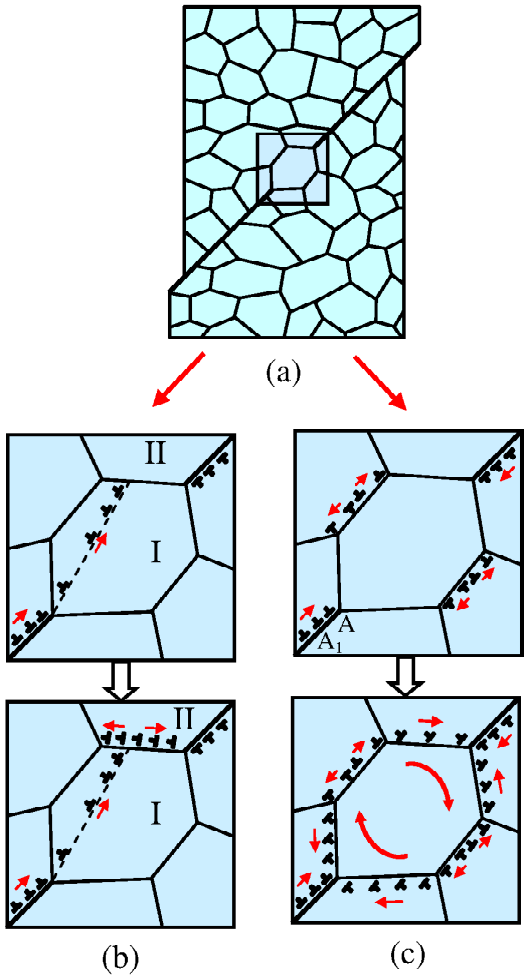

Fig. 1. Grain boundary sliding and its accommodation micromechanisms in a nanocrystalline specimen. (a) Grain boundary sliding occurs along grain boundaries and stops at triple junctions of grain boundaries. Grain boundary dislocations are accumulated at the grain boundaries near the triple junctions. (b) Lattice dislocations are emitted from a triple junction into a grain. They transform into grain boundary dislocations whose slow climb controls the rate of both dislocation emission from the triple junction and thereby grain boundary sliding. (c) Grain boundary sliding along grain boundary A_1A is accommodated by rotational deformation which involves slow climb of grain boundary dislocations and grain boundary sliding along neighboring grain boundaries.

(super)plastic deformation is effectively accommodated by emission of lattice dislocations from triple junctions into grain interiors, their glide across grains, absorption at GBs, transformation into GB dislocations and diffusion-assisted climb of GB dislocations [4,27–29] (Figs. 1a and 1b). In the situation under consideration, diffusion-assisted climb of GB dislocations serves as the rate controlling process which thereby crucially contributes to basic characteristics of (super)plastically deformed nano- and microcrystalline materials [4,27–29]. For instance, the accommodation mechanism (Figs. 1a and 1b) is treated to be responsible for strain rate sensitivity value of $m \approx 0.5$ in microcrystalline materials showing superplasticity [4,27,28]. In nanocrystalline materials, the same accommodation mechanism is modified due to nanoscale effects, and this modification leads to deviations of strain rate sensitivity from its "microcrystalline" value of $m \approx 0.5$ [29,30].

GB diffusion in vicinities of triple junctions can also directly accommodate GB sliding in nanomaterials [26,31]. In this situation, one can distinguish optimum ranges of parameters that characterize cooperative actions of GB sliding and GB diffusion, namely, the ranges of parameters at which tensile ductility of high-strength nanomaterials enhances [26]. Within these optimum ranges, stress-strain curves of nanocrystalline specimens have rather extended stages specified by a moderate strain hardening that suppresses plastic strain instabilities and, at the same time, does not initiate crack generation instabilities [26].

The third micromechanism capable of effectively accommodating GB sliding in nanomaterials is rotational deformation, plastic deformation accompanied by rotations of the crystal lattice within nanoscale grains [32–34] (Figs. 1a and 1c). In general, following experimental data [1,33,35–40], computer simulations [41,42] and theoretical models [32,43–46], crystal lattice rotations in nanograins are rather widespread in nanomaterials at plastic and superplastic deformation regimes. In particular, the rotational deformation mode often operates in nanomaterials in parallel with GB sliding; see [1–5] and references therein. In this context, it is logical to think that rotational deformation can serve as one of dominant accommodation micromechanisms for GB sliding on the nanoscale level. This view is indirectly supported by the fact that lattice slip is severely hampered in nanomaterials with finest grains [1,4,5,14], and thereby its role in GB sliding accommodation diminishes with decreasing grain size of a specimen. For instance, the number of lattice dislocations that can be emitted from a triple junction (Figs. 1a and 1b) dramatically decreases with decreasing grain size [29]. When this number is around 1 to 3, the effect of lattice dislocations within a grain is hardly significant compared to the effects of GB dislocations whose slip and climb carry rotational deformation.

Besides, the standard representations on accommodation of GB sliding through lattice dislocation emission from triple junctions [27–30] (Figs. 1a and 1b), in fact, are focused on the initial stage of plastic flow through GB sliding as the dominant deformation mode. GB sliding at this first stage can be divided into several elementary processes, each occurring in an isolated GB and its vicinity (Figs. 1a and 1b). In contrast to the standard representations, the idea of accommodation of GB sliding through rotational deformation is more relevant in description of the second deformation stage where GB sliding processes simultaneously occur in many GBs. At the second deformation stage, a grain of a deformed specimen typically has most its boundaries containing active GB dislocations that slip and/or climb along these boundaries, contributing to GB sliding and rotational deformation (Figs. 1a and 1c).

In most cases, in nanomaterials under quasistatic mechanical loading, rotational deformation is a slow, diffusion-controlled process [45]. Therefore, when GB sliding is accommodated by rotational deformation, the latter significantly or even crucially influences the behavior of nanomaterials during superplastic deformation and creep processes dominated by GB sliding. Gutkin et al. [32] and Bobylev et al. [34] theoretically described geometric and energy characteristics of rotational deformation as a process accommodating GB sliding. In particular, it was revealed that rotational deformation initiated by GB sliding represents an energetically favorable process in wide range of parameters of nanomaterials under plastic deformation. However, previous theoretical examinations [32,34] were not concerned with the kinetics of rotational deformation accommodating GB sliding in nanomaterials. (Bobylev et al. [34] suggested using a standard equation to describe plastic strain rate in microcrystalline materials, but in reality it is too rough to adequately take into account the specific features of deformation behaviors of nanomaterials deformed by cooperative GB sliding and rotational deformation processes.) At the same time, the kinetics of plastic deformation processes is of critical importance for calculation of stress-strain curves and other characteristics of materials during plastic and superplastic deformation tests. The main aims of this paper are to describe the kinetics of GB sliding and rotational deformation operating cooperatively, calculate the corresponding dependences of the flow stress on plastic strain and estimate values of plastic strain rate in nanocrystalline materials predominantly deformed by GB sliding accommodated by rotational deformation. Also, the effects of combined GB sliding and rotational deformation processes on ductility of nanomaterials will be discussed.

2. GRAIN BOUNDARY SLIDING AND DIFFUSION-CONTROLLED ROTATIONAL DEFORMATION IN NANOCRYSTALLINE MATERIALS. MODEL

Let us consider a nanocrystalline solid under a remote tensile load s. We focus our analysis on the situation where plastic flow in the solid occurs mostly through GB sliding accommodated by rotational deformation whose rate is controlled by GB diffusion. As it has been noted in Section 1, both GB sliding and rotational deformation effectively operate in nanocrystalline materials at superplastic and high-strain deformation regimes. During superplastic deformation, mesoscopic sliding surfaces – chains of GBs with approximately parallel planes – are often formed in nanocrystalline materials, and GB sliding occurs along them [47–49]. A mesoscopic sliding surface typically consists of several flat segments separated by grains whose geometry prevents GB sliding (Fig. 1a). These GB configurations of superplastic nanocrystalline materials serve as carriers of pronounced combined actions of GB sliding and rotational deformation [34]. Below we will theoretically examine this pronounced manifestation of GB sliding and rotational deformation in nanocrystalline structures.

Within our model, we consider a model hexagonal grain ABCDEF in a two-dimensional section of a nanocrystalline specimen where mesoscopic sliding surfaces, AA_1 and DD_1, are formed which are separated by the grain in question (Fig. 2). Let the boundaries of the grain have the same length *d*, and two GBs, BC and EF, are parallel with the mesoscopic sliding surfaces making an angle of 45° with the direction of the tensile load σ (Fig. 2). The applied load σ creates nonvanishing shear stresses at the mesoscopic sliding surfaces adjoining to the grain ABCDEF. These shear stresses initiate and drive GB sliding along the surfaces (Fig. 2).

Due to the approximately flat geometry of mesoscopic sliding surfaces, GB sliding along them is enhanced. GB sliding along the surfaces AA_1 and DD_1 is carried by GB dislocations which, for geometric reasons, are hampered at the triple junctions A and D, respectively (Fig. 2). Due to this hampering process, GB dislocation pile-ups are formed at the mesoscopic sliding surfaces. The

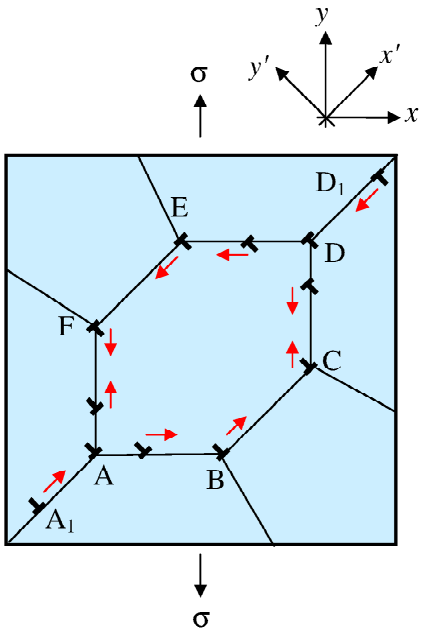

Fig. 2. Grain boundary sliding and dislocation climb in a model two-dimensional fragment of a nanocrystalline solid. Dislocations glide over grain boundaries A_1A and D_1D towards triple junctions A and D. After that they move (through climb and slip) along the boundaries of the hexagonal grain ABCDEF. Dislocations of opposite signs moving from triple junctions A and D, respectively, meet each other at grain boundaries CD and AF and eventually annihilate. Arrows indicate the directions of dislocation motion.

dislocation pile-ups serve as stress concentrators [34,50,51] and thereby provide a high level of local stresses near their heads, in particular, in the grain ABCDEF. The high stresses induce rotational deformation in the grain (Fig. 2). Thus, GB sliding and its accommodating rotational deformation occur cooperatively in a nanocrystalline specimen.

As to more details, let us consider evolution of GB dislocations reaching the triple junctions A and D due to GB sliding (Fig. 2). Under the action of the external load σ (concentrated at the GB dislocation pile-up heads), these dislocations climb over GBs AB and DE. Then new GB dislocations come to triple junctions A and D due to GB sliding. Under the action of both the applied load and the stresses of neighboring dislocations these dislocations climb over GBs AB, DE, AF, and CD, leaving the place for new sliding dislocations at the GB junctions A and D. In the course of plastic deformation this process repeats many times. When dislocations climbing over GBs AB and DE come to the points B and E, respectively, they start to slip over GBs BC and EF towards the junctions C and F. From the above junctions these dislocations climb over GBs CD and FA until they react with the opposite-sign dislocations climbing over the same GBs in opposite directions (Fig. 2). This GB dislocation evolution provides rotational deformation in the grain ABCDEF (Fig. 2).

The GB dislocations at triple junctions A and D hamper the glide of new dislocations to these junctions due to the dislocation-dislocation interaction, thereby resulting in strain hardening. At the same time, when GB diffusion is fast enough, these dislocations rapidly climb away from triple junctions A and D. In doing so, the dislocations react with dislocations of opposite sign and annihilate, thus reducing strain hardening. Thus, GB sliding along mesoscopic surfaces and diffusion-controlled rotational deformation (Figs. 1 (a and c) and 2) cause competing effects on strain hardening

In order to estimate the combined effects of GB sliding and rotational deformation on strain hardening in nanocrystalline solids, we have performed computer simulations of dislocation motion over GBs of the examined hexagonal grain (Fig. 2). The simulation procedure implemented is similar to the discrete dislocation dynamics approach but incorporates dislocation climb over GBs. Within our model, we postulate that new edge GB dislocations slip over mesoscopic sliding surfaces AA_1 and DD_1 due to intense GB sliding. These new GB dislocations appear at triple junctions A and D at regular time intervals determined by the specified strain rate $\dot{\varepsilon}$. Then the GB dislocations climb over GBs adjacent to the triple junctions (Fig. 2). In a first approximation, the climb velocity $v_c^{(k)}$ of the *k*-th GB dislocation is calculated using the formula [29,52] for the velocity of isolated dislocations climbing over an infinite flat GB as

$$v_c^{(k)} = \frac{D_{gb}}{R_s}\left|\exp\left(\frac{\sigma_{nn}^{(k)}\Omega}{k_B T}\right) - 1\right|, \qquad (1)$$

where D_{gb} is the GB self-diffusion coefficient, R_S is the dislocation screening length, $\sigma_{nn}^{(k)}$ is the component of the total stress tensor created at the core of the considered *k*-th climbing dislocation by the applied stress and other dislocations, $\boldsymbol{n}$ is the normal to the GB, Ω is the atomic volume, k_B is the Boltzmann constant, and T is the absolute temperature. The direction of dislocation climb along a GB is specified by the sign of the stress σ_{nn} and the sign of the climbing dislocation. For a GB dislocation with an elementary Burgers vector magnitude $b \approx 0.1$ nm, we put $R_S=2d$. In parallel with the applied load, the dislocation stresses

contribute to the total stress $\sigma_{nn}^{(k)}$. These stresses are calculated here for the case of an infinite isotropic solid characterized by the shear modulus G and Poisson ratio ν.

Let us introduce the coordinate system (x,y) as shown in Fig. 2. Then the stress $\sigma_{nn}^{(k)}$ in formula (1) is calculated as follows: $\sigma_{nn}^{(k)} = \sigma_{yy}^{(k)}$ for the points at the horizontal facets, AB and ED, of the examined grain ABCDEF, and $\sigma_{nn}^{(k)} = \sigma_{xx}^{(k)}$ for the points at the vertical facets, AF and CD, of the examined grain. In turn, the stresses $\sigma_{xx}^{(k)}$ are calculated as follows:

$$\sigma_{xx}^{(k)} = \sum_{\substack{j=1 \\ j\neq k}}^{N} s_j \sigma_{xx}^{d}(x_k - x_j, y_k - y_j), \tag{2}$$

$$\sigma_{yy}^{(k)} = \sigma + \sum_{\substack{j=1 \\ j\neq k}}^{N} s_j \sigma_{yy}^{d}(x_k - x_j, y_k - y_j), \tag{3}$$

where N is the number of climbing dislocations, σ is the applied load, as above, s_j is the (positive or negative) ratio of the projection of the Burgers vector of the j-th climbing dislocation onto the x-axis to the projection $b/\sqrt{2}$ of the elementary GB dislocation Burgers vector **b** ($b \approx 0.1$ nm), $\sigma_{xx}^{d}(x_k - x_j, y_k - y_j)$ and $\sigma_{yy}^{d}(x_k - x_j, y_k - y_j)$ are the stress components created by the j-th dislocation in the point (x_k, y_k) provided it has an elementary dislocation Burgers vector with the projection on the x-axis equal to $b/\sqrt{2}$.

The stress components $\sigma_{xx}^{d}(x,y)$ and $\sigma_{yy}^{d}(x,y)$ of the dislocation with the Burgers vector **b** = $(b/\sqrt{2})(\mathbf{e}_x + \mathbf{e}_y)$ (where $\mathbf{e}_x$ and $\mathbf{e}_y$ are the unit vectors directed along the x- and y-axis, respectively) are calculated using the expressions [50] for the stress field of a dislocation in an isotropic infinite solid as follows:

$$\sigma_{xx}^{d}(x,y) = \frac{D\left[b_y x\left(3y^2 + x^2\right) - b_x y\left(3x^2 + y^2\right)\right]}{\left(x^2 + y^2\right)^2}, \tag{4}$$

$$\sigma_{yy}^{d}(x,y) = \frac{D\left(b_x y + b_y x\right)\left(x^2 - y^2\right)}{\left(x^2 + y^2\right)^2}, \tag{5}$$

where $D = G/[2\pi(1 - \nu)]$, $b_x = b_y = b/\sqrt{2}$.

Also, in our simulations, we consider the possibility of dislocation coalescence. We assume that two GB dislocations coalesce, if their distance is smaller than the Burgers vector magnitude of an elementary GB dislocation. The velocities of non-elementary dislocations (resulting from coalescence processes) are assumed to be inversely proportional to their Burgers vector magnitudes. For simplicity, we do not consider splitting of non-elementary GB dislocations. Also, we suppose that, when dislocations reach junctions B and E, they very rapidly glide along nanoscale GBs BC and EF to the junctions C and F, respectively. With this assumption, in our simulations, the coalescence of gliding and climbing GB dislocations at the junctions C and F is considered, and GB dislocation distributions over the GBs BC and EF are neglected.

At every simulation time step, we calculate the velocities of all the dislocations (determined by the local normal stresses created by other dislocations and the applied load) and compute the new time step in such a way that the displacements of all the dislocations during this time step do not exceed some specified value. If a climbing dislocation passes the point B or E, it is automatically moved to the point C or F, respectively. If a climbing dislocation passes the point C or F, it is automatically moved to the point B or E, respectively.

The plastic strain ε resulting from GB dislocation motion under consideration serves as an important characteristic of the deformation processes in a nanocrystalline specimen. We roughly estimate the plastic strain as $\varepsilon \approx Nb/d$, where N is the number of dislocations that have slipped over GB AA_1. (Also, for symmetry reasons, N is equal to the number of dislocations that have slipped over GB DD_1). In these circumstances, plastic strain rate $\dot{\varepsilon}$ is given as $\dot{\varepsilon} \approx b/(\Delta t d)$, where Δt is the time interval between the moments of dislocation formation at triple junction A, and t is the deformation time ($\Delta t \approx t/N$ for $N >> 1$). Thus, the time interval Δt is expressed in terms of strain rate $\dot{\varepsilon}$ as $\Delta t = b/(\dot{\varepsilon} d)$.

In order to calculate the stress-strain dependence, we need to calculate the flow stress at every time interval Δt. In the following, we consider the shear flow stress t created by the applied load σ at GB AA_1. The shear stress τ is related to the tensile load σ by the relation $\tau = \sigma/2$. The flow stress τ is calculated as the critical (lowest) stress necessary for the energy-barrier-free motion of a GB dislocation from the junction A_1 towards the junction A. This stress corresponds to the case where the projection of the force acting on the dislocation at GB AA_1 (with the Burgers vector in the direction A_1A; see Fig. 2) in the direction A_1A is positive at any point of GB AA_1. The expression for τ is written as

$$\tau = \max\left\{\frac{\sigma_y}{2} - \sum_{k=1}^{N} s_k \sigma^{d}_{x'y'}(x - x_k, y - y_k),\ (x,y) \in A_1A\right\}, \quad (6)$$

where σ_y is the tensile yield stress of the simulated material. In formula (6) the Cartesian coordinate system (x',y') is chosen in such a way that the x'-axis is directed along the vector A_1A (see Fig. 2). The maximum in formula (6) is calculated numerically by calculating the expression in brackets in large enough number of points of the GB A_1A and choosing the maximum of the calculated values. The initial stress τ at the time $t = 0$ is set equal to $\sigma_y/2$.

3. RESULTS OF SIMULATIONS

Using the above simulation procedure, we have calculated the stress-strain dependences, for nanocrystalline Ni and Al_2O_3. In the case of Ni, we used the following parameter values: d = 20 nm, G = 79 GPa [53], ν = 0.31 [53], $\Omega = 1.094\times10^{-29}$ m^3 [53], σ_y = 0.8 GPa [54], T = 350K and $D_{gb} = D_{gb0}\exp[-Q/(RT)]$, where $D_{gb0} = 1.8\times10^{-12}$ m^{2}s^{-1} [55], Q = 46 KJ/mol [55], and R = 8.31 J/(mol K) is the universal gas constant. For Al_2O_3, we exploited the following parameter values: d = 20 nm, G = 169 GPa [56], ν = 0.23 [56], $\Omega = 0.87\times10^{-29}$ m^3 [56], σ_y = 0.2 GPa, T = 1200K, D_{gb0} = 2 m^{2}s^{-1} [57] and Q = 400 KJ/mol [57].

The dependences of the flow shear stress τ on the plastic strain ε, for nanocrystalline Ni and nanocrystalline ceramic α-Al_2O_3, are presented in Fig. 3a and 3b, respectively, at various values of strain rate $\dot{\varepsilon}$. As it is seen, for the high enough strain rate of $\dot{\varepsilon} = 5\times10^{-3}$ s^{-1}, GB sliding and associated accumulation of GB dislocations near triple junctions A and D lead to dramatic strain hardening at the initial deformation stage. As a result, the flow stress τ reaches high values of 2 GPa, for Ni, and 3.5 GPa, for Al_2O_3, at low plastic strain of ε = 0.01. At the same time, for the comparatively low strain rate of $\dot{\varepsilon} = 10^{-4}$ s^{-1}, the flow stress rapidly grows up to values of around 1.2 GPa, for Ni, and of 0.8 to 1 GPa, for Al_2O_3. Then, strain hardening stops, and the flow stress is approximately constant with further increase in plastic strain. The flow stress saturates in nanocrystalline Ni and Al_2O_3, because these materials during deformation at $\dot{\varepsilon} = 10^{-4}$ s^{-1} rapidly reach their dynamic equilibrium states in which the strain hardening effect of GB sliding (that produces accumulation of GB dislocations at triple junctions which stop GB sliding) is completely compensated by the strain softening effect of diffusion-controlled rotational deformation (that leads to annihilation of GB dislocations).

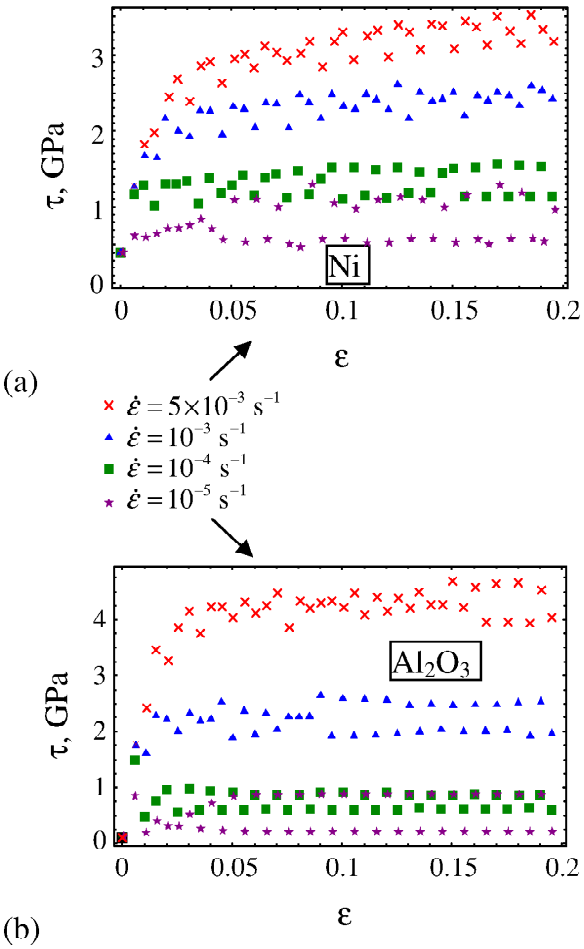

Fig. 3. Dependence of the flow shear stress τ on plastic strain ε for the deformed nanocrystalline Ni (a) and Al_2O_3 (b) under uniaxial tensile loading, for d = 20 nm, T = 350K (a) and 1200K (b) and various values of strain rate $\dot{\varepsilon}$.

It should be noted that the simulated values of the flow stress oscillate with ε, especially in the case of low $\dot{\varepsilon}$. These oscillations are related to the details of the simulation procedure. More precisely, within our model, we consider only plastic flow in one grain and its vicinities, in which case the calculated flow stress τ at a specified time moment strongly depends on the precise positions of climbing dislocations at this moment. For instance, according to our simulations of plastic flow in one grain and its vicinities at low $\dot{\varepsilon}$ (e.g., $\dot{\varepsilon} = 10^{-5}$ s^{-1}), the number of dislocations near triple junctions A and D is small (typically 1 or 2), and the local flow stress is highly sensitive to their positions. In the

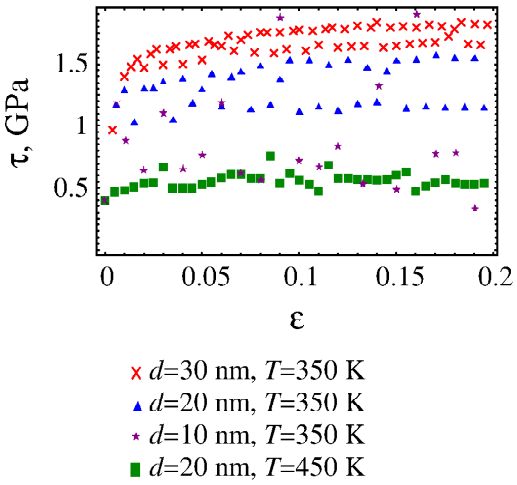

Fig. 4. Dependences of the flow shear stress τ on plastic strain ε for nanocrystalline Ni at various grain sizes *d* and deformation temperatures *T*.

case of high strain rate, the number of dislocations in the vicinities of triple junctions A and D is large enough, and the precise positions of dislocations exert small influence on the local flow stress. As a result, in this case, the oscillations of the flow stress have low amplitudes. These oscillations should disappear if one considers GB sliding and rotational deformation processes occurring simultaneously in multiple grains and calculate the flow stress as an average of the local flow stresses for various grains.

Based on the calculated stress-strain dependences, one can estimate strain rate sensitivity, $m = \partial \ln\tau / \partial \ln\dot{\varepsilon}$, serving as an important parameter specifying plastic flow in solids. According to our calculations for nanocrystalline Ni and Al_2O_3, values of *m* are typically in the range from 0.1 to 0.4 for Ni and from 0.1 to 0.6 for Al_2O_3, when plastic strain rate $\dot{\varepsilon}$ is within the interval from 10^{-5} s^{-1} to 5×10^{-3} s^{-1}. These values are of the same order as those (> 0.33) typical for conventional superplasticity exhibited by microcrystalline and ultrafine-grained materials at elevated temperatures.

The general trend of the calculated $m(\varepsilon)$ dependence for nanocrystalline Ni and Al_2O_3 is that *m* increases with rising plastic strain ε, for low values of ε, and is nearly constant, for large enough values of ε (at which the flow stress τ weakly varies with ε; see, e.g., the curves corresponding to $\dot{\varepsilon} = 10^{-4}$ s^{-1} in Figs. 3a and 3b). Also, *m*, on average, decreases with a decrease in strain rate $\dot{\varepsilon}$. These two trends are associated with the fact that, for low strains and/or high strain rates, diffusion does not have enough time to significantly change dislocation positions and therefore exerts an inessential effect on the flow stress τ. Also, the calculated values of *m* oscillate with ε due to the previously discussed oscillations of the flow stress $\tau(\varepsilon)$.

In addition to the sensitivity to $\dot{\varepsilon}$, the flow stress shows the sensitivity to both temperature *T* and grain size *d*. Fig. 4 presents the dependences $\tau(\varepsilon)$ for nanocrystalline Ni at various values of grain size *d* and deformation temperature *T*. As it follows from Fig. 4, the flow stress τ decreases with an increase in temperature *T* and/or decrease in grain size *d*. This behavior is related to the trends that the rate of GB dislocation climb grows with rising temperature, and the annihilation rate of climbing dislocations at GBs increases with diminishing grain size.

As it has been noted above, for high enough values of ε and low enough values of $\dot{\varepsilon}$, a nanocrystalline solid under a mechanical load reaches a dynamic equilibrium state characterized by low strain hardening or its absence. We attribute this equilibrium state to a balance between the strain hardening effect of GB sliding and the strain softening effect of diffusion-controlled rotational deformation. In terms of GB dislocations, a dynamic equilibrium state corresponds to the situation where climbing GB dislocations are distributed over GBs and rapidly annihilate with dislocations of opposite signs. In doing so, intense annihilation processes prevent accumulation of sliding GB dislocations near triple junctions A and D. In order to illustrate this statement, Fig. 5 presents GB dislocation configurations in nanocrystalline Ni deformed at plastic strain rate of $\dot{\varepsilon} = 10^{-4}$ s^{-1}, for various values of plastic strain ε. As it is seen in Fig. 5, for $\varepsilon < 0.05$, the populations of GB dislocations near triple junctions A and D rapidly increase with rising plastic strain (see Figs. 4a and 4b). (Also, note that the numbers of dislocations at GBs AB and DE are larger than those at GBs AF and CD. This difference is due to the action of the applied stress which increases the rate of dislocation climb over horizontal GBs compared to that over vertical GBs.) With a further increase in plastic strain ε (see Figs. 5c and 5d), the populations of GB dislocations near triple junctions A and D just weakly increase. Also, with an increase in ε, one can observe the accumulation of the dislocation charges at junctions C and F, associated with the difference of dislocation climb rates over horizontal and vertical GBs. In spite of this aspect, dislocations of opposite signs climbing over GBs CD and AF react and eventually annihilate. The dislocation annihilation hinders the accumulation of large dislocation charges near triple junctions A and D and thereby impedes dramatic strain hardening.

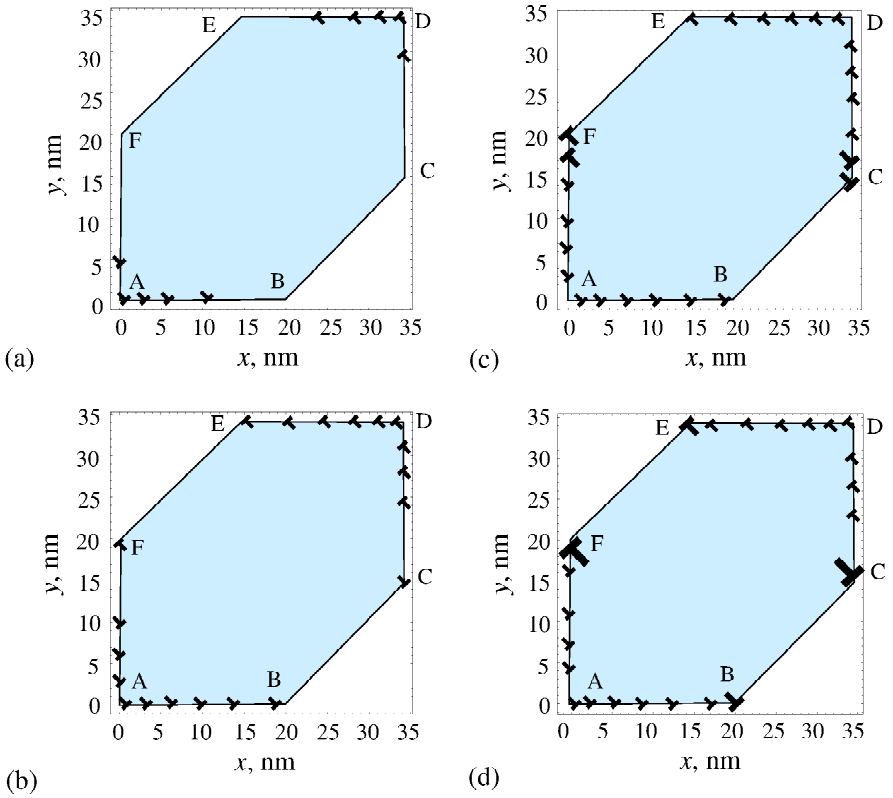

Fig. 5. Dislocation configurations at grain boundaries of a model hexagonal grain ABCDEF in deformed nanocrystalline Ni at $\dot{\varepsilon} = 10^{-4}$ s^{-1}, ε =0.025 (a), 0.05 (b), 0.1 (c) and 0.2 (d). The sizes of dislocations signs are proportional to the magnitudes of their Burgers vectors.

In the previous consideration, we have considered the case of plastic flow with a constant strain rate. In parallel with this case, we have also simulated the situation of creep, where plastic deformation occurs under the action of a constant tensile load σ that creates a constant shear stress $\tau = \sigma/2$ in the plane making the angle of $\pi/4$ with the loading direction. To simulate the creep case, we assumed that dislocation can glide to the corners A and D of the examined grain over GBs A_1A and D_1D if the shear stress τ exceeds the critical shear stress for this process (calculated as described above). The dependences of strain rate $\dot{\varepsilon}$ on strain ε for nanocrystalline Ni are presented in Fig. 6, for the case of d = 20 nm, T = 350K and various values of stress τ (Fig. 6a) as well as for the case of the specified stress τ = 1 GPa and various values of grain size d and absolute temperature T (Fig. 6b). Fig. 6a demonstrates that at small values of strain ε, strain rate $\dot{\varepsilon}$ decreases. This is associated with dislocation accumulation near the corners A and D of the examined grain, which hinders plastic flow. At larger strains, strain rate, although oscillates, stays on average constant. This is associated with the annihilation of dislocations of opposite signs at the GBs of the examined grain, which prevents further dislocation accumulation near the corners A and D. Fig. 6a also demonstrates the evident fact that strain rate $\dot{\varepsilon}$ increases with the flow stress τ. Also, as it follows from Fig. 6b, strain rate $\dot{\varepsilon}$ increases as grain size d decreases or/and temperature T increases.

4. DISCUSSION

The dependences $\tau(\varepsilon)$ presented in Fig. 3 are indicative of the following behavioral features of nanocrystalline materials (Ni and Al_2O_3) deformed cooperatively by GB sliding and diffusion-controlled rotational deformation.

(i) The flow stress-strain dependences at comparatively high strain rates of $\dot{\varepsilon} = 5\times10^{-3}$ and 10^{-3} s^{-1} are characterized by both dramatic strain hardening at the initial deformation stage and high values of the ultimate shear stress. Such shear stresses can occur only at local regions near powerful stress concentrators/sources. For instance, GB dislocation pile-ups can be formed at mesoscopic sliding surfaces and create very high local stresses in grains near pile-up heads, that is, grains where rotational deformation is realized. Strain hardening inherent to nanocrystalline materials

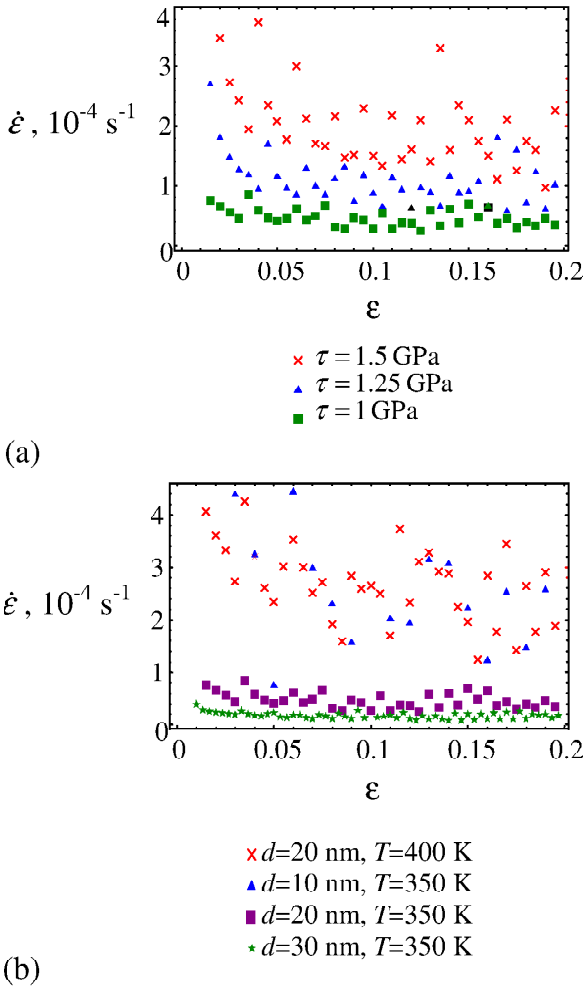

Fig. 6. Dependence of the strain rate $\dot{\varepsilon}$ on plastic strain ε for deformed nanocrystalline Ni under uniaxial tensile loading, for (a) d=20 nm, T=350K and various values of τ; and (b) τ = 1 GPa and various values of grain size d and temperature T.

deformed at high strain rates of $\dot{\varepsilon} = 5\times10^{-3}$ and 10^{-3} s^{-1} (Fig. 3) suppresses plastic strain instability at least for plastic strain $\varepsilon \le 0.05$ and thus enhances tensile ductility of these materials. After the initial stage, the second deformation stage takes place (Fig. 3). It is characterized by an approximately constant level of the flow stress with no strain hardening. At the same time, plastic flow of nanocrystalline Ni and Al_2O_3 at both the initial and second deformation stages is specified by rather high values of strain rate sensitivity ($m = \partial \ln\tau / \partial \ln\dot{\varepsilon}$) ranging from 0.1 to 0.4, for Ni, and from 0.1 to 0.6, for Al_2O_3. These values are of the same order as those (> 0.33) typical for conventional superplasticity exhibited by microcrystalline and ultrafine-grained materials at elevated temperatures. Thus, when nanocrystalline Ni is deformed cooperatively by GB sliding and rotational deformation, it is characterized by a rather high strain rate sensitivity which enhances its tensile ductility.

(ii) The flow stress-strain dependences of nanocrystalline materials (Ni and Al_2O_3) deformed at comparatively low strain rates of $\dot{\varepsilon} = 10^{-4}$ and 10^{-5} s^{-1} are characterized by a nearly constant flow stress (Fig. 3). (Its values in the case of Ni are typical for real nanocrystalline specimens under an external load even if powerful stress concentrators are absent. For instance, these values are close to those documented in experiments with tensile deformation of nanocrystalline Ni-15%Fe alloy [58].) That is, the deformation stage with pronounced strain hardening is in fact absent at such strain rates. At the same time, as with nanocrystalline Ni deformed at high strain rates, plastic flow of nanocrystalline Ni at comparatively low strain rates is specified by rather high values of strain rate sensitivity m ranging from 0.1 to 0.4. With these values of m, one expects enhancement of tensile ductility for nanocrystalline Ni deformed cooperatively by GB sliding and rotational deformation.

5. CONCLUDING REMARKS

In this paper, a model was suggested describing the kinetics of GB sliding and its accommodating rotational deformation in nanocrystalline materials. Within the model, GB sliding initiates and is accommodated by rotational deformation occurring, in its turn, through GB sliding and diffusion-controlled climb of GB dislocations (Figs. 1(a and c) and 2). That is, GB sliding plays a double role as a process which simultaneously initiates and conducts rotational deformation. Rotational deformation also plays a double role as a process that simultaneously accommodates GB sliding and has it as its constituent process (Figs. 1(a and c) and 2).

We performed computer simulations of cooperative GB sliding and rotational deformation processes in a nanocrystalline specimen (Figs. 1(a and c) and 2). As a result, we calculated the dependences of the flow stress on plastic strain in nanocrystalline Ni and Al_2O_3 (Fig. 3) as well as estimated typical values of strain rate sensitivity m of nanocrystalline Ni in the situation where GB sliding and diffusion-controlled rotational deformation serve as the dominant deformation modes. The dependences presented in Fig. 3, in particular, show that nanocrystalline Ni and Al_2O_3 deformed at comparatively high strain rates of $\dot{\varepsilon} = 5\times10^{-3}$ and 10^{-3} s^{-1} are characterized by pronounced strain hardening at the initial deformation stage and nearly

constant high values of the flow shear stress at the second deformation stage. Strain hardening at the initial deformation stage suppresses plastic strain instability and thereby enhances tensile ductility of nanocrystalline materials under examination. In the case of deformation at sufficiently low strain rate and/or high temperatures, intense GB diffusion decreases the flow stress level and can slow down or, possibly, completely eliminate strain hardening. Also, we found that plastic flow of nanocrystalline Ni and Al_2O_3 loaded at low and high strain rates is specified by rather high values of strain rate sensitivity (ranging from 0.1 to 0.4, for Ni, and from 0.1 to 0.6, for Al_2O_3, in the examined intervals of strain rate and temperature). With these values of *m*, nanocrystalline Ni deformed cooperatively by GB sliding and rotational deformation tends to exhibit enhanced tensile ductility. This theoretically revealed deformation behavior is well consistent with experimental data on tensile deformation of nanocrystalline Ni and Ni-Fe15% alloy [58,59].

ACKNOWLEDGMENTS

The work was supported, in part, by the Russian Ministry of Education and Science (Grant 14.B25.31.0017, Contract 8025 and grant MD-164.2012.1), St. Petersburg State University research grant 6.37.671.2013, and the Russian Foundation of Basic Research (grant 12-01-00291-a).

REFERENCES

[1] A.K. Mukherjee // *Mater. Sci. Eng.* A **322** (2002) 1.
[2] M. Dao, L. Lu, R.J. Asaro, J.T.M. De Hosson and E. Ma // *Acta Mater.* **55** (2007) 4041.
[3] A. Mukhopadhyay and B. Basu // *Int. Mater. Rev.* **52** (2007) 257.
[4] M. Kawasaki and T.G. Langdon // *J. Mater. Sci.* **42** (2007) 1782.
[5] C.C. Koch, I.A. Ovid'ko, S. Seal and S. Veprek, *Structural Nanocrystalline Materials: Fundamentals and Applications* (Cambridge, Cambridge University Press, 2007).
[6] A.S. Khan, B. Farrok and L. Takacs // *J. Mater. Sci.* **43** (2008) 3305.
[7] A.S. Khan, B. Farrok and L. Takacs // *Mater. Sci. Eng.* A **489** (2008) 77.
[8] E.C. Aifantis // *Mater. Sci. Eng.* A **503** (2009) 190.
[9] C.S. Pande and K.P. Cooper // *Progr. Mater. Sci.* **54** (2009) 689.
[10] S.V. Bobylev, A.K. Mukherjee, I.A. Ovid'ko and A.G. Sheinerman // *Int. J. Plasticity* **26** (2010) 1629.
[11] B. Farrokh and A.S. Khan // *Int. J. Plasticity* **25** (2009) 715.
[12] H.A. Padilla II and B.L. Boyce // *Exp. Mechanics* **50** (2010) 5.
[13] I.A. Ovid'ko // *Mater. Phys. Mech.* **12** (2011) 76.
[14] I.A. Ovid'ko and A.G. Sheinerman // *Rev. Adv. Mater. Sci.* **29** (2011) 105.
[15] I.A. Ovid'ko and A.G. Sheinerman // *Rev. Adv. Mater. Sci*. **27** (2011) 189.
[16] I.A. Ovid'ko, A.G. Sheinerman and E.C. Aifantis // *Mater. Phys. Mech.* **12** (2011) 1.
[17] F. Cleri // *Int. J. Plasticity* **37** (2012) 31.
[18] J. Li and A.K. Soh // *Int. J. Plasticity* **39** (2012) 88.
[19] N.F. Morozov, I.A. Ovid'ko, A.G. Sheinerman and N.V. Skiba // *Rev. Adv. Mater. Sci.* **32** (2012) 75.
[20] I.A. Ovid'ko and T.G. Langdon // *Rev. Adv. Mater. Sci*. **30** (2012) 103.
[21] I.A. Ovid'ko and A.G. Sheinerman // *Rev. Adv. Mater. Sci*. **32** (2012) 61.
[22] B. Wang, H. Idrissi, M. Galceran, M.S. Colla, S. Turner, S. Hui, J.P. Raskin, T. Pardoen, S. Godet and D. Schryvers // *Int. J. Plasticity* **37** (2012) 140.
[23] L. Zhu and J. Lu // *Int. J. Plasticity* **30-31** (2012) 166.
[24] K.S. Kumar, S. Suresh, M.F. Chisholm, J.A. Norton and P. Wang // *Acta Mater.* **51** (2003) 387.
[25] I.A. Ovid'ko and A.G. Sheinerman // *Acta Mater.* **52** (2004) 1201.
[26] I.A. Ovid'ko and A.G. Sheinerman // *Acta Mater.* **57** (2009) 2217.
[27] O.A. Ruano, J. Wadsworth and O.D. Sherby // *Acta Mater.* **51** (2003) 3617.
[28] T.G. Langdon // *J. Mater. Sci.* **41** (2006) 597.
[29] F.A. Mohamed and M. Chauhan // *Metall. Mater. Trans.* A **37** (2006) 3555.
[30] F.A. Mohamed // *Metall. Mater. Trans.* A **38** (2007) 340.
[31] I.A. Ovid'ko and A.G. Sheinerman // *Acta Mater.* **53** (2005) 1347.
[32] M.Yu. Gutkin, I.A. Ovid'ko and N.V. Skiba // *Acta Mater.* **51** (2003) 4059.
[33] Y.B. Wang, B.Q. Li, M.L. Sui and S.X. Mao // *Appl. Phys. Lett.* **92** (2008) 011903.
[34] S.V. Bobylev, A.K. Mukherjee and I.A. Ovid'ko // *Rev. Adv. Mater. Sci.* **19** (2009) 103.

[35] M. Ke, W.W. Milligan, S.A. Hackney, J.E. Carsley and E.C. Aifantis // *Nanostruct. Mater.* **5** (1995) 689.
[36] M. Murayama, J.M. Howe, H. Hidaka and S. Takaki // *Science* **295** (2002) 2433.
[37] Zh. Shan, E.A. Stach, J.M.K. Wiezorek, J.A. Knapp, D.M. Follstaedt and S.X. Mao // *Science* **305** (2004) 654.
[38] I. Zizak, N. Darowski, S. Klaumunzer, G. Schumacher, J.W. Gerlach and W. Assmann // *Phys. Rev. Lett.* **101** (2008) 065503.
[39] S. Cheng, Y. Zhao, Y. Wang, Y. Li, X.-L. Wang, P.K Liaw and E.J. Lavernia // *Phys. Rev. Lett.* **104** (2010) 255501.
[40] P. Liu, S.C. Mao, L.H. Wang, X.D. Han and Z. Zhang // S*cripta Mater.* **64** (2011) 343.
[41] T. Shimokawa, A. Nakatani and H. Kitagawa // *Phys. Rev.* B **71** (2005) 224110.
[42] I. Szlufarska, A. Nakano and P. Vashista // *Science* **309** (2005) 911.
[43] I.A. Ovid'ko // *Science* **295** (2002) 2386.
[44] M.Yu. Gutkin and I.A. Ovid'ko, *Plastic Deformation in Nanocrystalline Materials* (Springer, Berlin, 2004).
[45] I.A. Ovid'ko and A.G. Sheinerman // *Scripta Mater.* **59** (2008) 119.
[46] I.A. Ovid'ko, A.G. Sheinerman and E.C. Aifantis // *Acta Mater.* **56** (2008) 2718.
[47] J. Markmann, P. Bunzel, H. Roesner, K.W. Liu, K.A. Padmanabhan, R. Birringer, H. Gleiter and J. Weissmueller // *Scripta Mater.* **49** (2003) 637.
[48] A.V. Sergueeva, N.A. Mara, N.A. Krasilnikov, R.Z. Valiev and A.K. Mukherjee // *Philos. Mag.* **86** (2006) 5797.
[49] A.V. Sergueeva and A.K. Mukherjee // *Rev. Adv. Mater. Sci.* **13** (2006) 1.
[50] J.P. Hirth and J. Lothe, *Theory of Dislocations* (Wiley, New York, 1982).
[51] A.A. Fedorov, M.Yu. Gutkin and I.A. Ovid'ko // *Acta Mater.* **51** (2003) 887.
[52] J. Friedel, *Dislocations* (Pergamon Press, Oxford, 1964).
[53] C.J. Smithells and E.A. Brands, *Metals Reference Book* (Butterworth, London, 1976).
[54] W.M. Yin, S.H. Whang, R. Mirshams and C.H. Xiao // *Mater. Sci. Eng.* A **301** (2001) 18.
[55] Yu.R. Kolobov, R.Z. Valiev and M.B. Ivanov, *Grain Boundary Diffusion and Properties of Nanostructured Materials* (Cambridge Int. Sci. Publ., Cambridge, 2007).
[56] R.G. Munro // *J. Am. Ceram. Soc.* **80** (1997) 1919.
[57] A.G. Evans, J.R. Rice and J.P. Hirth // *J. Am. Ceram. Soc.* **63** (1980) 368.
[58] H. Li and F. Ebrahimi // *Appl. Phys. Lett.* **84** (2004) 4307.
[59] H. Li and F. Ebrahimi // *Adv. Mater.* **17** (2005) 1969.